LDEF METEOROID & DEBRIS SPECIAL INVESTIGATION GROUP INVESTIGATIONS AND ACTIVITIES AT THE JOHNSON SPACE CENTER

Thomas H. See
Lockheed Engineering & Science Co.
Houston, Texas 77058
(713) 483-5027 / FAX (713) 483-5347

Michael E. Zolensky
NASA / Johnson Space Center
Houston, Texas 77058
(713) 244-5128 / FAX (713) 483-5347

Ronald P. Bernhard
Lockheed Engineering & Science Co.
Houston, Texas 77058
(713) 483-5018 / FAX (713) 483-5347

Jack L. Warren
Lockheed Engineering & Science Co.
Houston, Texas 77058
(713) 483-5122 / FAX (713) 483-5347

Clyde A. Sapp
Lockheed Engineering & Science Co.
Houston, Texas 77058
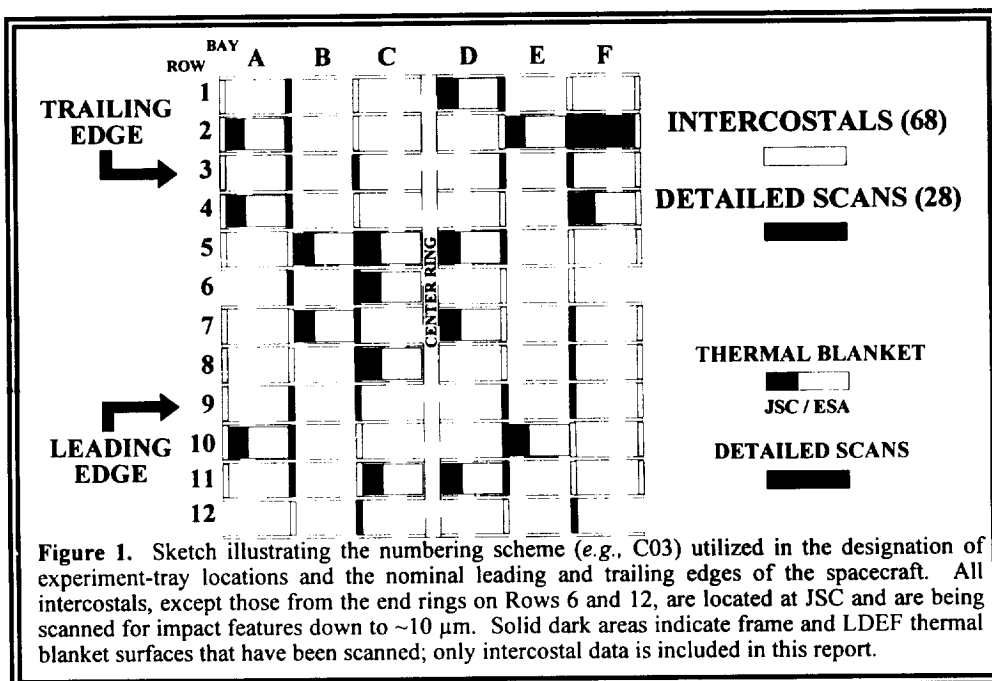(713) 483-5141 / FAX (713) 483-5347

Claire B. Dardano
Lockheed Engineering & Science Co.
Houston, Texas 77058
(713) 483-5329 / FAX (713) 483-5347

INTRODUCTION

Since the return of the Long Duration Exposure Facility (LDEF) in January, 1990, members of the Meteoroid and Debris Special Investigation Group (M&D SIG) at the Johnson Space Center (JSC) in Houston, Texas have been examining LDEF hardware in an effort to expand the knowledge base regarding the low-Earth orbit (LEO) particulate environment. In addition to the various investigative activities, JSC is also the location of the general Meteoroid & Debris database. This publicly accessible database contains information obtained from the various M&D SIG investigations, as well as limited data obtained by individual LDEF Principal Investigators.

LDEF exposed ~130 m² of surface area to the LEO particulate environment, ~15.4 m² of which was occupied by structural frame components (*i.e.*, longerons and intercostals) of the spacecraft. The data reported here was obtained as a result of detailed scans of LDEF intercostals, 68 of which reside at JSC (Figure 1). The limited amount of data presently available on the A0178 thermal control blankets was reported last year (ref. 1) and will not be reiterated here. As was the case in Ref. 1, the data presented here are limited to measurements of crater diameters and their frequency of occurrence (*i.e.*, flux).

Since our last report

Figure 1. Sketch illustrating the numbering scheme (*e.g.*, C03) utilized in the designation of experiment-tray locations and the nominal leading and trailing edges of the spacecraft. All intercostals, except those from the end rings on Rows 6 and 12, are located at JSC and are being scanned for impact features down to ~10 µm. Solid dark areas indicate frame and LDEF thermal blanket surfaces that have been scanned; only intercostal data is included in this report.
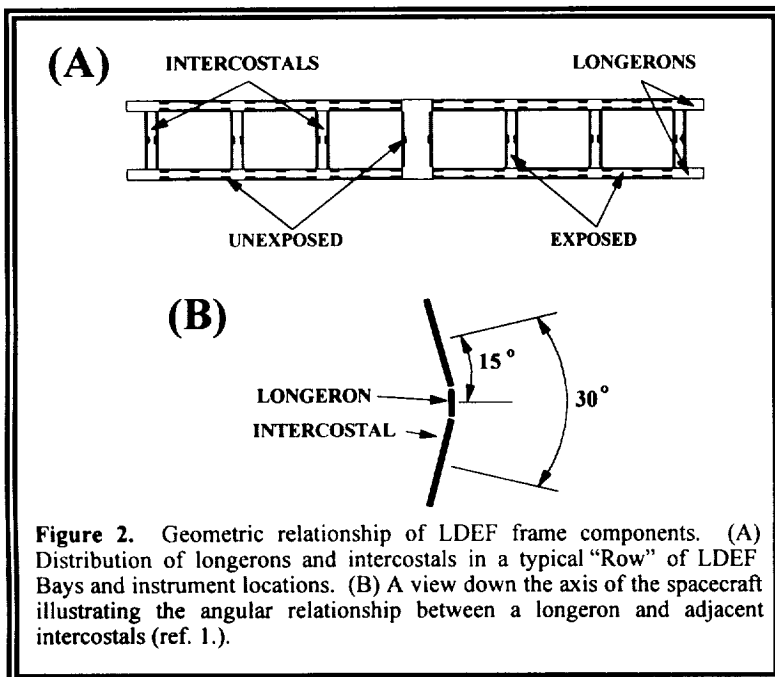
(ref. 1) we have scanned another 14 intercostals and now have detailed information on at least two intercostals from each of LDEF's 12 rows. In addition, we have scanned two more intercostals each from Rows 3 and 9 for a total of 28 intercostals.

RATIONALE FOR EXAMINING LDEF'S STRUCTURAL FRAME

The size of a crater or penetration hole depends on the physical properties of the target and projectile materials, and on the projectile's mass and impact velocity. On LDEF, a given impactor would generate craters of different sizes depending on the location or pointing direction of the target because of the different encounter velocity, assuming a constant target material. The quantitative relationships for these parameters are known for some LDEF materials, but only over a restricted range and set of initial conditions. Because of the M&D SIG's desire to determine particle frequencies as a function of pointing direction it was necessary to characterize impact features on identical target materials so that the physical properties of the target remain constant. Furthermore, because of the highly stochastic nature of the collisional environment, it is also necessary to study materials which exposed sufficient surface areas to have accumulated a representative population of impact features. Finally, it was necessary to select surfaces which could be made available to the M&D SIG for study. Few surfaces on LDEF met such criteria. The A0178 Teflon thermal blankets were not present on Rows 3, 9 and 12, although they did expose ~20 m² of surface area to the LEO particulate environment; one third of each blanket is curated at JSC. In addition, the majority of impact features on these surfaces were penetrations and not craters. Lastly, the penetration and/or cratering behavior of this material is not presently well understood, although such studies are now underway (ref. 2). Another set of candidate surfaces was the 25 Meteoroid & Space Debris Impact Experiment trays (S0001; exposing ~26.3 m² of aluminum) that were located on every row of LDEF (including the space and Earth ends) except for Row 9. These various factors pointed to LDEF's structural frame as the best candidate surfaces to fit all of these criteria.
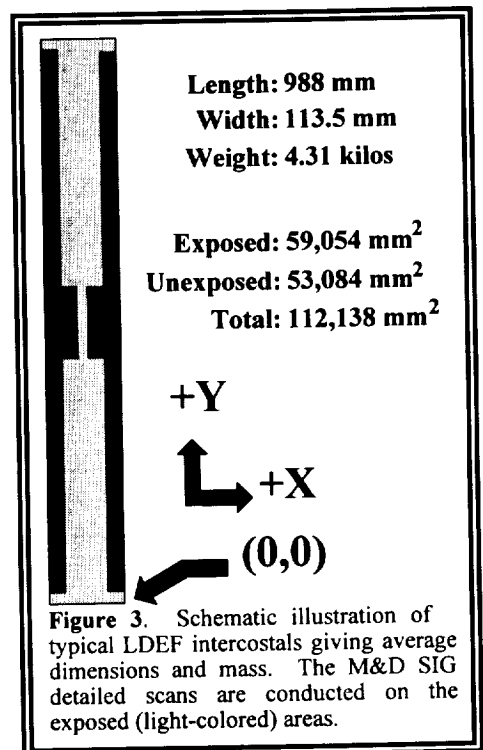
LDEF's entire structural frame was fabricated from 6061-T6 aluminum, a commonly used spacecraft material whose response to hypervelocity impact has been studied in great detail (e.g., refs. 3, 4, and 5). The frame components formed an open-grid, 12-sided structure that produced individual instrument bays (Bays A-F; Figure 1) and provided attachment points for the experiment trays. The longitudinal frame members (~4.6 m long) were termed "longerons" (Figure 2a), while cross members between longerons were called "intercostals" (~1 m in length; Figures 2a and 3). Individual rows were assigned

Figure 2. Geometric relationship of LDEF frame components. (A) Distribution of longerons and intercostals in a typical "Row" of LDEF Bays and instrument locations. (B) A view down the axis of the spacecraft illustrating the angular relationship between a longeron and adjacent intercostals (ref. 1.).

258

sequential numbers (1-12), with Row 9 facing in the nominal velocity vector (leading-edge direction) and Row 3 in the trailing-edge direction. For more detailed information regarding the numbering scheme utilized by the M&D SIG interested readers are referred to Refs. 1 and 6. Because of their size and mass, and because of their significance to the overall structural integrity of the spacecraft, the longerons and the components from the Earth- and space-facing ends could not be made available for detailed study in the laboratory. On the other hand, the small size and mass, as well as the higher than average surface polish, made the intercostals well suited for removal and detailed scanning within the Facility for the Optical Inspections of Large Surfaces (FOILS) laboratory at JSC.
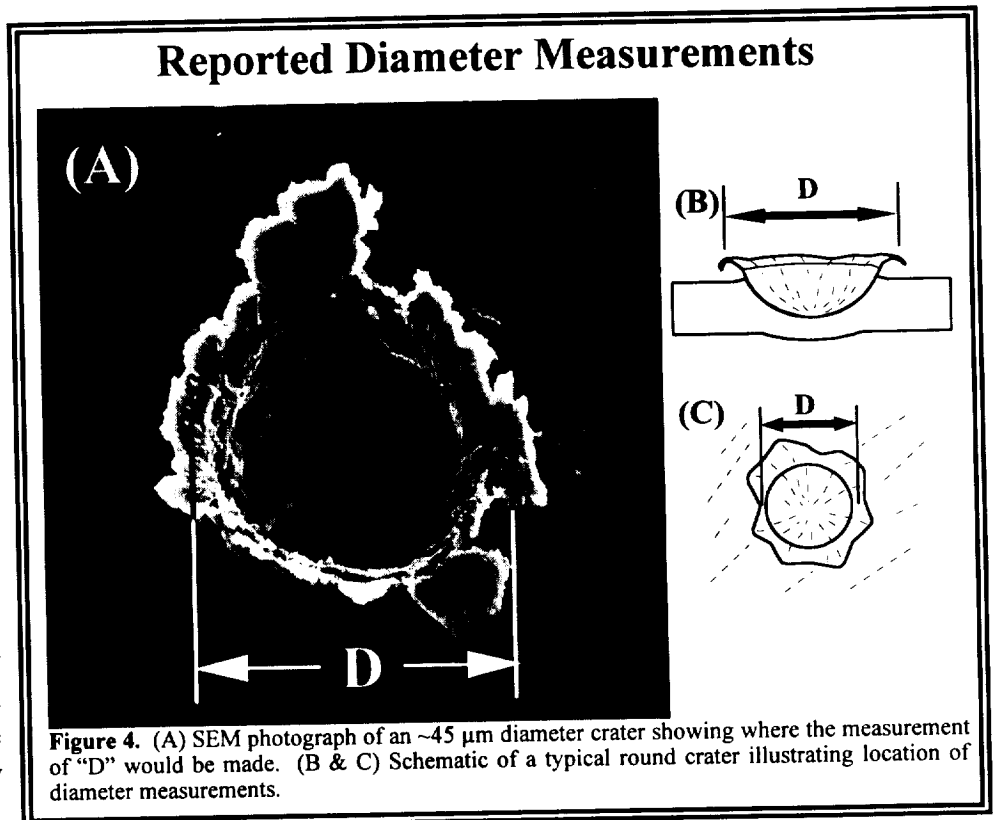
SURFACE AREAS AND PROCEDURES

Length: 988 mm
Width: 113.5 mm
Weight: 4.31 kilos

Exposed: 59,054 mm²
Unexposed: 53,084 mm²
Total: 112,138 mm²

+Y

+X

(0,0)

Figure 3. Schematic illustration of typical LDEF intercostals giving average dimensions and mass. The M&D SIG detailed scans are conducted on the exposed (light-colored) areas.

Each intercostal exposed ~0.06 m² of surface area to the LEO particulate environment (Figure 3), while a complete row of intercostals, not including the center ring (*i.e.*, the four mid and two end-ring intercostals; see Figures 1 and 2), totaled ~0.32 m²; end-ring intercostals exposed only ~0.04 m² each. Multiply by 12 and subtracting the two Row 6 and two Row 12 intercostals not included results in a total exposed surface area for the 68 intercostals of ~3.68 m², ~1.65 m² of which are included in this report.

As has been our practice throughout our LDEF investigations, reported crater diameters refer to rim-crest-to-rim-crest dimensions (Figure 4). For a detailed discussion on the crater morphology and associated measurement techniques for craters in aluminum, as well as impacts into other materials that were on LDEF, interested readers should see Refs. 6 and 7.

Table 1 lists the number of impact craters, sorted by size, documented in our study, as well as the exposed surface areas which have been examined on each row

Reported Diameter Measurements

(A)

D

(B) |← D →|

(C) |← D →|

Figure 4. (A) SEM photograph of an ~45 μm diameter crater showing where the measurement of "D" would be made. (B & C) Schematic of a typical round crater illustrating location of diameter measurements.

259

C-4

thus far. All scanning was carried out within the FOILS laboratory at JSC; the intercostals were scanned at a 40x magnification which easily permits the identification of all craters >30 µm in diameter on the relatively smooth intercostal surfaces. *Thus, for craters below ~40 µm in diameter the coverage is not complete.*

Table 1. Number of individual features documented in each size bin for the 12 LDEF rows as determined from the detailed scans of the intercostals, along with the associated exposed surface area for each row. Size bins are inclusive on the lower end of each bin (*i.e.*, bin 10 contains all particles ≥10 µm and <14 µm in diameter.

LDEF Row Number	<10	10	14	20	28	40	57	80	113	160	226	320	453	640	905	1280	1810	2560	3620	5120	TOTALS	LDEF Row Number	Surface Area (m²; exposed)
Row 1				3	6	16	15	14	7	6	3	1									71	Row 1	0.118650
Row 2				10	14	12	11	14	3	3	1	1									69	Row 2	0.117385
Row 3			2	6	6	15	13	9	6	7	4	3	1	1							73	Row 3	0.232544
Row 4				1	1	6	8	7	4	4	1	1	1			1					35	Row 4	0.120025
Row 5		1	5	34	16	12	8	6	6	4	1	1	1	1							96	Row 5	0.118361
Row 6	1		2	17	28	42	11	10	9	10	5	1	3	1							140	Row 6	0.119976
Row 7	1	41	61	236	150	106	27	36	21	21	11	6	2	1							720	Row 7	0.117871
Row 8				10	45	83	46	46	33	20	16	16	2	2	1						320	Row 8	0.117433
Row 9		12	15	98	114	195	117	108	73	57	34	15	12	5	1	1					857	Row 9	0.234776
Row 10				22	59	90	57	55	41	29	18	7	13	3	2						396	Row 10	0.118871
Row 11	1	1	8	67	70	106	46	50	25	24	9	7	3	1		1	1				420	Row 11	0.119729
Row 12		2	6	33	36	60	29	32	22	9	9	2	2								242	Row 12	0.119334
TOTALS		57	99	537	545	743	388	387	250	194	112	60	39	17	4	3	1				3439	TOTALS	1.654955

ANALYTICAL RESULTS

Impact Frequency

One of the goals of the M&D SIG is to determine the impact frequency of natural meteoritic and man-made particles on LDEF. To date, a limitation in resources has prevented an extensive effort along these lines at JSC; there are several reasons for this. First, the actual samples are far too large to be accommodated by a Scanning Electron Microscope (SEM) and/or Microprobe without putting forth a considerable effort to section the intercostals via an end-mill. Second, the composition of the target material (*i.e.*, aluminum) makes identification of man-made aluminum impactors virtually impossible; aluminum is known to constitute a significant fraction of the man-made particle population. Lastly, other metallic surfaces, such as the A0187-1 99.99% pure gold meteoroid detectors (ref. 8), revealed that nearly half of all craters analyzed do not contain sufficient quantities of projectile residue to permit detection and classification of the impactor, whether meteoritic or man-made, via SEM techniques. As a result, the focus of this intercostal investigation has been to simply determine the frequency with which LDEF was impacted by all particle types and how the frequency varied from row to row (*i.e.*, pointing direction), and not to determine the percentages of craters formed by either natural or man-made particles.

To gain an *estimate* of the original projectile diameter from the measured crater diameter in metallic surfaces, M&D investigators commonly assume that the resulting crater is on the order of four to five times larger than the diameter of the projectile. We could do this also, but choose not to for the following reasons. As mentioned earlier, the size of a crater in a given target material not only depends on the physical properties of the target and projectile, but also on the projectile's velocity. On LDEF, not only

did the average encounter velocity vary as a function of pointing direction, it also varied depending on whether the projectile was man made or natural; in general, natural particles possess higher encounter velocities than do man-made particles (refs. 3 & 4). Thus, with so many unknowns, any attempt to determine particle-type frequency would result in flux curves with extremely large degrees of uncertainty.
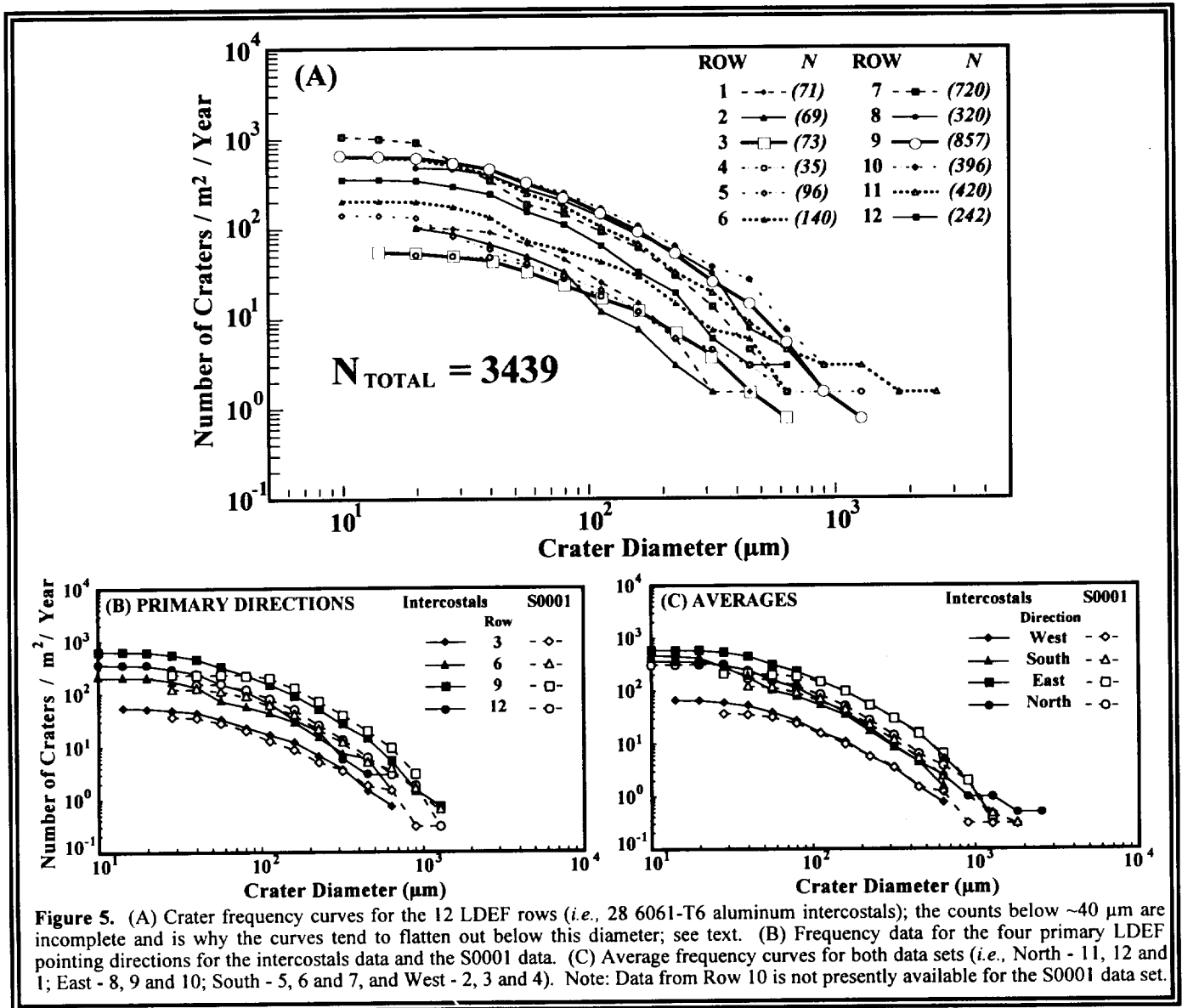

Figure 5. (A) Crater frequency curves for the 12 LDEF rows (*i.e.*, 28 6061-T6 aluminum intercostals); the counts below ~40 μm are incomplete and is why the curves tend to flatten out below this diameter; see text. (B) Frequency data for the four primary LDEF pointing directions for the intercostals data and the S0001 data. (C) Average frequency curves for both data sets (*i.e.*, North - 11, 12 and 1; East - 8, 9 and 10; South - 5, 6 and 7, and West - 2, 3 and 4). Note: Data from Row 10 is not presently available for the S0001 data set.

Figure 5a displays the crater frequencies for the 28 intercostals examined to date. In general, the additional data acquired over the past year have done little to alter our interpretations and have mainly served to improve the overall fidelity of the data. These data continue to be in good agreement with our earlier results (ref. 1), as well as that of others (*e.g.*, ref. 9), with the highest cratering rates being observed in the forward-facing directions (*i.e.*, Rows 8, 9 and 10) and the lowest frequencies being found in association with the rearward-facing surfaces (*i.e.*, Rows 2, 3 and 4).

Over the past year D. Humes (Langley Research Center [LaRC]) has forwarded copies of his S0001 experiment data to the M&D SIG for inclusion in the M&D Database. At least one S0001 experiment tray was present on each of LDEF's 12 rows, except for Row 9; S0001 also occupied at least one bay on the

Earth- and space-ends of LDEF. Because of Row 9's importance, Humes acquired several aluminum surfaces from the S0010 experiment (Bay B09) from W. Slemp (LaRC). These data are also included in the M&D database.

Comparison of the M&D SIG intercostal and the Humes S0001 data sets can be seen in Figure 5b, where only the four major pointing directions are plotted for the sake of clarity. For most surfaces, Humes did not attempt to document craters below ~80 μm in diameter (Humes, personal communications), which accounts for the flattening of his flux curves below this diameter. For the intercostal data, we believe the data to be complete down to ~40 μm diameter craters, which is where the intercostal flux curves begin to flatten out. In addition, Humes includes data for all crater sizes, including those that were previously documented at the Kennedy Space Center by the M&D SIG A-Teams (ref. 6). On average, Humes' diameter measurements for the same craters tend to be on the order of 8% to 12% larger than the KSC reported diameter. This may account for the minor differences seen between the cratering frequencies plotted in Figure 5b, which are in generally good agreement for identical pointing direction. As can be seen, the S0001 data tends to exhibit slightly higher cratering frequency (above his cutoff diameter of ~100 μm) for all directions except Row 3, the trailing-edge direction.

Like Figure 5b, Figure 5c again compares these two extensive data sets. In this figure, however, the frequency curves represent averages (i.e., East represents the average flux for Rows 8, 9 and 10; S0001 Row 10 data not included at this time) for the four cardinal pointing directions (e.g., North [Row 12], East [Row 9], etc.) of LDEF. When this averaging is done to both data sets, the differences between the two become negligible, particularly for the East- and West-facing directions; for the West-facing direction the two curves lie right on top of each other between 100 to 1000 μm diameter craters (Figure 5c).

Leading-Edge To Trailing-Edge Ratios

In general, the slopes for the various flux curves in Figures 5a - 5c are very similar, suggesting that the overall ratios of large to small particles remain relatively constant, regardless of LDEF pointing direction. Of greater interest are the relative production rates between the leading- and trailing-edges of LDEF. Prior to LDEF's recovery, it was believed that the leading-edge surfaces would receive ~20 times more impacts per unit surface area than the trailing-edge surfaces (ref. 4). However, both the intercostal data and that of the S0001 experiment seem to indicate that the pre-LDEF estimates of these ratios were too high.

In Figure 6a, the intercostal data (solid bars) exhibits the maximum leading-edge to trailing-edge ratio of ~10:1 for craters ≥40 μm in diameter. What is also noticeable is that this ratio appears to decrease as crater size increases, reaching a minimum of ~7:1 for craters ≥640 μm in diameter. The S0001 data (open bars), although possessing higher absolute leading-edge to trailing-edge ratios, exhibits a similar trend ranging from a maximum of ~15:1, for craters ≥113 μm in diameter, to ~10:1 for craters ≥905 μm in diameter. (Recall that the S0001 data is only 100% complete for craters above 100 μm in diameter, while the intercostal data is believed to be 100% inclusive for craters down to ~40 μm in diameter). The average leading-edge to trailing-edge ratio for the two data sets is ~9:1 for the intercostals and ~12:1 for the S0001 surfaces.

Figure 6b represents the ratios of the forward-facing surfaces (i.e., Rows 8, 9 and 10) to those of the rearward-facing direction (i.e., Rows 2, 3 and 4). As was the case for the frequency data depicted in Figure 5, the differences between the two data sets all but disappear when the data are averaged in this fashion, both sets yielding an average forward-facing to rearward-facing ratio of ~8:1. In addition,

262

although it is not nearly as pronounced as in the Row 9 to Row 3 data of Figure 6a, the decrease in the forward-facing to rearward-facing ratio for the larger size craters is still apparent, reaching a minimum of ~5:1 for craters ≥905 in diameter for both sets of data.

Last year when we first noted this trend we pointed out that the number of craters ≥500 μm in diameter was extremely small (~2%), when compared to the ≥10 μm in diameter crater populations for intercostals on Rows 3 and 9. However, since that time we have tripled the scanned surface area for Row 3, and doubled the scanned surface area for Row 9. With these greatly improved counting statistics we find little change in the percentage (*i.e.*, ~3%) of craters ≥500 μm in diameter for Rows 3 and 9; as for the overall LDEF intercostal crater population ≥10 μm in diameter, the percentage of craters ≥500 μm in diameter is ~11.1%. For the S0001 data this percentage is ~6.5% for Rows 3 and 9, and ~11.3% for all S0001 surfaces examined to date. Nevertheless, this change in leading-edge to trailing-edge ratio as a function of crater size appears to be real. Additional evidence for such a change can be found in the thermal-blanket and MAP (ref. 10) experiment data illustrated in Figure 5c of Ref.

Figure 6. (A) Leading-edge to trailing-edge (*i.e.*, Row 9:3) ratios for the intercostal and S0001 data sets. (B) Similar ratios for the two data sets except that the forward-facing direction represents the average for Rows 8, 9 and 10, while the rearward-facing direction represents the average for Rows 2, 3 and 4.

1. For the larger penetration features (~500 μm in diameter) the leading- to trailing-edge ratio is ~10:1, while for the smallest features for which data is available on both Rows 3 and 9 (*i.e.*, ~5 μm in diameter) the leading-edge to trailing-edge ratio climbed to ~50:1. Although some of these effects may be related to the projectile sources, and hence the associated velocities of the different particle-population sizes, it does appear as though the larger particle population may be slightly more isotropically distributed.

The measured ratios, Row 9 to Row 3, of the spatial density of impact craters do not agree with current theoretically predicted ratios for either meteoroids (ref. 11) or for Earth-orbital debris (ref. 12). It follows that the present theoretical models are inadequate to explain the data (ref. 13). For meteoroids to produce a front-to-back ratio as low as 7:1, a much larger fraction of high-velocity meteoroids than previously modeled seems to be required. If orbital debris is the primary source for the observed impact craters, the data suggest that there is much more debris in geosynchronous transfer orbits than is currently included in models -- especially those with orbital inclinations near 28.5° (ref. 12). It appears as though a careful reexamination of such models (for incorrect assumptions) is in order.
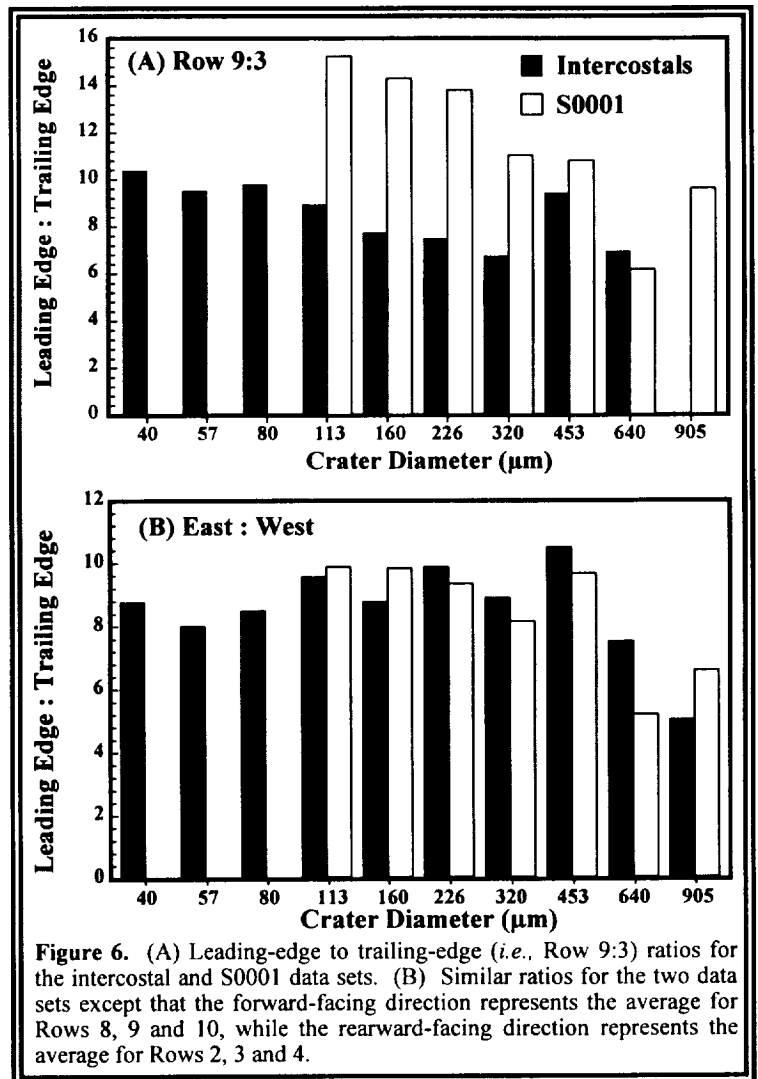
High-magnification optical examination of intercostal F07F02 has revealed an anomalous number of craters on this intercostal, the majority of which are ≤40 μm in diameter. In an effort to understand this phenomena and to identify the source of these features, the M&D SIG has analyzed (*i.e.*, Scanning Electron Microscopy / Energy Dispersive X-ray Analysis [SEM-EDX]) 251 of the 540 (~46%) impacts on intercostal F07F02. The objective of these examinations was to evaluate the chemical variability and possible clustering of discrete particle types and, hopefully, determine their source(s). Craters containing detectable projectile residues were classified as either micrometeoritic or as man-made debris, while sources of surface contamination were identified when ever possible.
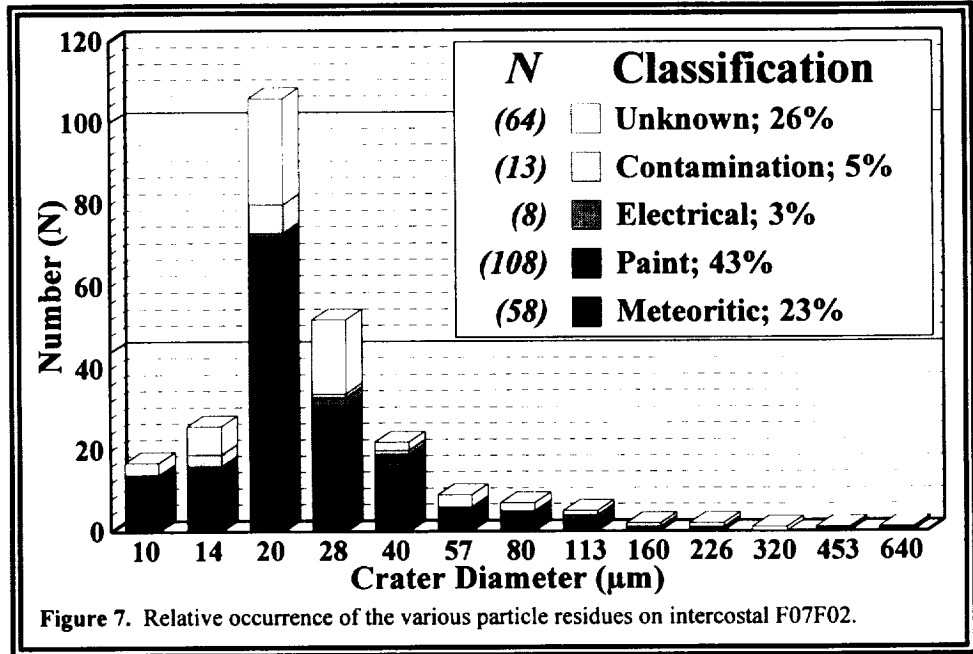

Figure 7. Relative occurrence of the various particle residues on intercostal F07F02.

The occurrence of the various projectile types has been tabulated in histogram form and is illustrated in Figure 7, which displays the relative frequencies of micrometeoritic, man-made debris particles (*i.e.*, paint and electrical components), indeterminate, and contamination samples for the smaller size bins. Examination of Figure 7 illustrates the trend toward a high occurrence of all particle types in the 14 to 40 μm size range, especially in the ≥20 μm to <28 μm size bin which contains ~63% of the analyzed craters. There is a particular increase in the relative amount of paint-type residues as compared to residues found on the gold surfaces from experiment A0187-1 and the experiment tray clamps (refs. 8 & 14, respectively). SEM characterization of the crater morphologies shows that the depth to diameter ratios, the crater rim characteristics, and the residue remnants are similar within this suite of impact features as those found within these other studies. The SEM-EDX spectra of the chemical residues associated with the majority of the impacts formed by paint-flake particles indicate that the paint was a Si, Cl, Ti-rich paint low in Zn (see Figure 8). Such data suggest that the paint type may have been Chemglaze A-276, or a paint of similar composition.
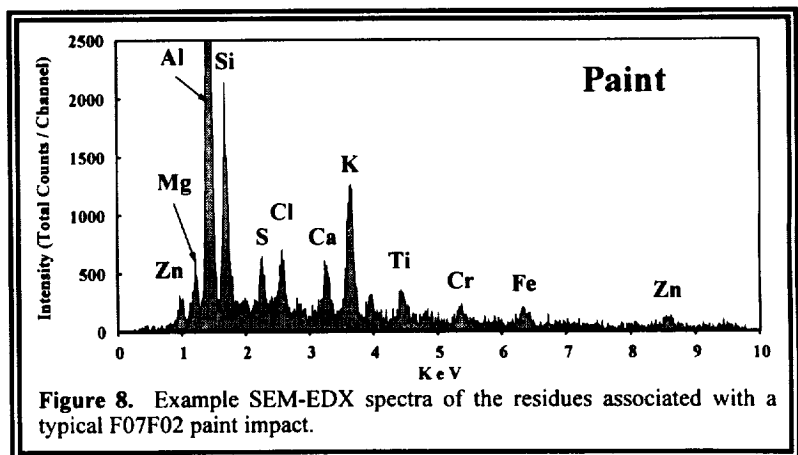

Figure 8. Example SEM-EDX spectra of the residues associated with a typical F07F02 paint impact.

STS-41C, the LDEF deployment mission in 1984, was also the Solar Maximum Satellite repair mission. Analysis of returned Solar Max hardware revealed that Chemglaze A-276, and similar paints which possessed organic binders, do not hold up well under long exposures in LEO (ref. 15). In short, the organic binders in these types of paint were readily broken down or eroded by atomic oxygen. As a result, spacecraft manufacturers today utilize paints with non-organic binders whenever possible.

Returning to intercostal F07F02, the anomalous increase in craters has not, to date, been documented on any other LDEF hardware, with the exception of the S0001 experiment-tray lips which were in direct contact with intercostal F07F02 (Humes, personal communications). Intercostal C07F02, from the other end of Row 7, does not exhibit this phenomenon, nor do intercostals in the same area of LDEF on adjacent rows on either side of Row 7. The similar chemical composition indicates that the projectiles originated from a common source. Photographs of LDEF have been examined in an effort to locate an object which could have served as a location for a primary impact that could have generated a large number of secondary craters on this intercostal. No such source is evident. Secondly, the particles may have been traveling as a dense cloud or group of orbital debris, yet this too seems unlikely considering the tightly packed or dense nature of the apparent debris swarm. Since neither of the previous sources seems likely, it appears as though these particles may have been Shuttle derived, originating during a primary impact into some Shuttle hardware (e.g., Remote Manipulator System [RMS], within the cargo bay, etc.), during either deployment or retrieval of LDEF.

Future Scanning Efforts

Members of the M&D SIG at JSC will continue to gather data from the detailed scans of the LDEF intercostals as long as funding permits. In related matters, the past year saw the return of the EURECA spacecraft, as well as the Hubble Space Telescope (HST) repair mission. The M&D SIG has already acquired sections of EURECA's thermal insulation materials which are presently being scanned at LaRC by D. Humes. Prior to the HST repair mission the M&D SIG had requested pieces of the return solar panels for examination. However, during the repair activities one of the two solar panels would not completely fold to a configuration permitting its return to Earth, and thus, was jettisoned over the side of the Shuttle. Whether or not the M&D SIG will still acquire any of this material for examination has yet to be determined. Nevertheless, LDEF will serve as the baseline or snap shot of the LEO particulate environment for the time period of April, 1984 to January, 1990. Future data will be compared to the data acquired from LDEF to evaluate how the LEO particulate environment is evolving with time.

3-DIMENSIONAL IMAGE ANALYSIS

Image Collection

During the three-month deintegration of LDEF, the M&D SIG generated ~4,500 digital, color stereo-image pairs of impact related features from all space-exposed surfaces, the idea being to reduce these images to yield more accurate feature information (e.g., crater depth and diameter with respect to the original target surface). In an earlier paper (ref. 16) we described the theory and practice of determining

this 3-dimensional feature information from stereo imagery, while a second paper (ref. 17) described some of the problems and solutions encountered during development of the algorithm that would be used to garner such information.

Initial Analysis Plan

Initial economic and portability constraints were the main factors involved in the decision to utilize stereo imagery as a means for extracting 3-D information from LDEF impact craters. The initial analysis plan was to perform automated, full-image windowed cross-correlation to determine a high resolution surface morphology of the crater images. Several problems (*e.g.*, specular reflectivity) encountered during the initial phases of the analysis demonstrated the impracticality of such an approach (ref. 17).

Our next approach was to use a parametric definition of the crater geometries using manually selected tie-points. A tie-point is a pair of points, one from each of the two images, which represent the same point on a surface (*i.e.*, a tie-point "ties" two images together at a single point). This approach made the assumption that crater geometries could be accurately defined by a paraboloid. It was eventually determined via a series of tests performed on a set of cross-sectioned craters (ref. 17) that a 2nd order (paraboloid) 3-D curve was not accurately describing the crater geometries adequately. Further analysis revealed that a 6th order curve resulted in a fairly accurate representation for the cross-sectioned profile of typical, experimentally derived impact craters.

6th Order Fit Decision

In order to perform a least-squares, 3-D 6th order curve fit on the stereo images, a much larger set of data points was required than for the 2nd order curve fits. This was a significant problem because of the man-hour intensive tie-point collection process, and because -- frequently -- the operator was unable to locate sufficient tie-points to perform the analysis. A technique was developed which utilized the initial tie-points (which had previously been collected for the paraboloid estimation) as "seeds" for a local area modified cross-correlation. These seed tie-points were used to center small search regions within the image over which to perform a modified cross-correlation search for more tie-points to be used as inputs to the 6th order curve fit.

AVODE Filter

The majority of the impact craters we were utilizing involved materials with a high degree of specular reflectivity (*i.e.*, aluminum). The effect of this reflectivity is to cause large differences in the photometric intensity of areas on the surfaces as observed from each camera due to the change in viewing angles with a stereo microscope. This meant that it was not feasible to perform traditional correlation techniques which assume that equivalent areas will appear equivalent on both images. In order to compensate for this problem the images were pre-filtered using an AVODE (Absolute Value Omni-Directional Edge) algorithm which was developed specifically for this purpose. The output from this filter is an image in which each pixel has encoded within it eight, 1-bit flags which indicate whether an edge exists in each of the primary eight directions. Note that these flags do not indicate the sign of the edge (bright to dark or dark to bright), nor do they indicate the magnitude of the edge. Neither of those traits is particularly relevant when dealing with specularly reflective materials. The advantages of this filter are that it leaves out irrelevant information and permits cross-correlation of the resultant images using a logical XNOR,

which is fairly CPU inexpensive. An XNOR is a bitwise operation which returns a 1 if the two inputs are the same and a 0 if they are different. The measure of agreement in a correlation is then just the sum of the bits in the output from the XNOR operation.

Iterative Photometric Calibration

One of the problems (and a lesson learned) with the original data collection was that the video-camera pairs, which were assigned to individual stereo-microscope systems (see ref. 6), were not photometrically calibrated prior to data acquisition. Unfortunately, this resulted in a significant difference in the photometric responses of the individual cameras, and forced us to perform an iterative, localized photometric calibration, which was incorporated into the AVODE filtering. It was not possible to perform a straightforward gain correction because of the reflectivity of the material.

Bi-directional Logical XNOR Correlation

After the input regions were processed through the AVODE filter, a windowed, logical XNOR cross-correlation was performed. This involves selecting a small reference area in one image and measuring its correlation with each possible location in the region of interest on the other image. The maximum correlation is then given a confidence value based on the sum of the bits in the XNOR output, the likelihood of the step size as compared to other surrounding tie-points, and the total number of bits turned on in the input regions. This last check is necessary to guard against areas with no edges correlating exactly.

After some experimentation it was determined that a bi-directional correlation drastically added to the trustworthiness of the results. This step consisted of swapping the reference and search images, and repeating the entire correlation process. Agreements between the two correlation passes give a much higher confidence to the resultant tie-points (*i.e.*, if A points to B and B points to A then it's much more likely that A & B form a valid tie-point than if A points to B, and B points to C).

Tie-Point Selection

The output of the bi-directional cross-correlation is an array of "best guess" tie-points with their corresponding confidence values. From this array is selected a subset of tie-points which pass a set of acceptance criteria. These new tie-points are then used as inputs to the 6th order surface solver. Note that the entire correlation process is performed separately for the internal crater surface and for the ambient plane.

Simplex Solution Of Crater Geometry

After several approaches were attempted, the final method used in solving for the coefficients of the 6th order curve was a downhill simplex algorithm (ref. 18). The benefits of this approach are that it is fairly simple to implement and modify, it requires only function evaluations (not derivatives), and it permits the addition of solution constraints (*e.g.*, ensuring that the center of the crater is the lowest point). This technique was also adapted to solve for the equation of the ambient plane.

Depth And Diameter Determination

Once the coefficients for the 6th order curve and ambient plane equations have been determined, the crater depth and diameter are calculated. The crater depth is defined as the distance between the ambient plane and the center (*i.e.*, bottom) of the 6th order curve. The crater diameter is defined as the diameter of the circle formed by the intersection of the ambient plane and the 6th order curve.

Error Estimation

In order to estimate the accuracy of the final results a Monte Carlo analysis was performed. This analysis consists of repeatedly adding random errors to the initial inputs and processing the results through the same algorithm as the original data. The random error is normally distributed about zero with the standard deviation based on the residuals of the initial curve fit. A large number of passes through this process were performed and a statistical analysis of the resultant outputs was used to estimate the accuracy of the initial fit.

Description Of Test Craters And Manual Measurements

To determine the overall accuracy and reliability of the analysis system described above, a set of eight test craters were carefully measured. For this purpose, eight >300 µm in diameter craters were chosen from various aluminum LDEF tray clamps. Binocular images of these craters were then collected in the FOILS Laboratory at JSC, utilizing the same type system and parameters that were employed in gathering the stereo-image pairs during LDEF deintegration. Seed tiepoints were collected for these image pairs in preparation for processing.

Tuneable Parameters

A total of 37 different parameters within the various data-reduction routines were determined to be "tuneable" (*i.e.*, parameters whose settings could affect the overall accuracy and reliability of the analysis algorithm). An example of a tuneable parameter is the size of the reference area to be used. All parameters were initially set at what were felt to be reasonable values and all eight test craters processed. Ideally, a 37-dimensional array of results would have been generated, and the best settings for all parameters would be defined as the point in that array which gave the most accurate results. Due to time, intelligence, and CPU limitations, however, it was decided to make the assumption that the effects of each of the tuneable parameters were independent (at least to first order) and each parameter was individually adjusted while leaving all other parameters at a fixed value. Multiple passes of this process eventually resulted in a set of values for the tuneable parameters which gave the most accurate results. Each run of the analysis software not only outputs an estimate of the crater depth and diameter, but an estimate of the potential error associated with those results. A significant portion of the parameter tuning involved attempting to minimize these errors while maximizing the trustworthiness of the error analysis (*i.e.*, ensuring that the true answer lay between the error bars).

When the tuning had been completed, a 90% trustworthiness was achieved with semi-acceptable error bars. Unfortunately, when the overall analysis routine was applied to a subset of the unknown images, the error estimates were unacceptably large (less than 25% of the unknown craters that were processed possessed error-bar ranges of less than 10%) as to make any studies based on the results futile. After an

268

extensive effort it was decided to abort any further attempts to improve the analysis results of these stereo-image pairs, mainly because of the poor initial image quality (*e.g.,* lack of photometric calibration, extremely narrow depth of field, synchronization problems during digitization, etc.).

<center>3-Dimensional Image Acquisition; Lesson Learned</center>

As a result of the efforts made in attempting to reduce the stereo-image pairs acquired at KSC by the M&D SIG, there are several key parameters and/or conditions which should be addressed before any such future efforts are undertaken. By addressing these issues up front, much of the work needed to reduce the data could be eliminated. These issues are:

1) A photometric calibration should be performed on the entire image acquisition system prior to data collection to ensure similar photometric response between the two images.

2) A method for increasing the depth-of-field of the optical system needs to devised.

3) The orientation and type of lighting utilized at image acquisition needs to be investigated (*e.g.,* a 360° ring lighting may give better results than spot lighting).

4) The intensity of the light source should be increased over what was utilized by the M&D SIG, or use more sensitive video cameras, or both. This may also enable the aperture to be closed down, and aid with the depth-of-field problems.

5) Image "noise" must be minimized. This can be accomplished by averaging a sequence of images, or by increasing the light and turning down the camera gain.

<center>## MISCELLANEOUS M&D SIG ACTIVITIES AT JSC</center>

With FY 94 bringing to a close the initial investigative phases of LDEF, the M&D SIG is active on several fronts in consolidating information and attempting to make it available for future use by M&D workers and spacecraft engineers.

<center>M&D Database</center>

In a continuing effort to make all M&D data available to the general user community, the M&D SIG at JSC is constantly updating the M&D Database with data from all possible sources, including data generated at JSC, as well as data provided by various LDEF investigators. At the time of this writing the database contained detailed information on more than 16,000 individual impact features that have been documented on LDEF. A little more than half of this data has been generated by direct M&D SIG

activities and investigations, while the remainder has been provided by various LDEF investigators. However, the M&D SIG would like to receive more data from any and all potential sources and are requesting that anyone having such data please forward it to T.H. See or M.E. Zolensky. Details regarding the format of such information should be discussed with either T.H. See and/or C.B. Dardano.

Access to, and use of the data contained within the M&D Database is encouraged. In addition, although FY 1994 will bring to a close the initial and intensive LDEF investigation, the M&D Database at JSC will continue to serve as a repository for M&D type data. Therefore, M&D investigators are encouraged to continue to send such data for inclusion with this extensive M&D Database. The M&D Database is accessible via any of the following techniques.

A) DECNET: 1) Log onto host computer.
2) Type SET HOST 9300.
3) Type PMPUBLIC at *Username:* prompt.

INTERNET: 1) Type TELNET 146.154.11.35
or
TELNET CURATE.JSC.NASA.GOV
2) Type PMPUBLIC at *Username:* prompt.

MODEM: The modem may be 300, 1200, or 2400 baud; no parity; 8 data bits; 1 stop bit. The area code is 713 for long distance calls.
1) Dial 483-2500.
2) Type SN_VAX in response to the *Enter Number:* prompt.
3) Hit <CR> 2 or 3 times after the *CALL COMPLETE* message.
4) Type J31X in response to the # prompt.
5) Type C CURATE in response to the *Xyplex>* prompt.
6) Type PMPUBLIC at the *Username:* prompt.

Periodic updates on the state of the JSC holdings of LDEF, as well as other meteoroid-related activities, are issued by the Office of the Curator at JSC in the form of the *Dust Courier*. Parties interested in being added to the distribution list of this publication should contact M.E. Zolensky.

LDEF-Related Images On CD-ROM

Presently, members of the M&D SIG at JSC are actively involved in the curation and distribution of various photographic images related to the deployment, retrieval and post-retrieval documentation of LDEF. Already in progress at JSC is the transfer of the ~4,500 stereo images of various LDEF impact features that were taken during the initial deintegration and examination of LDEF at the Kennedy Space Center, as well as all of the subsequent images acquired at JSC. All of these images have been converted into a TIFF file format and are being transferred on to CD-ROM. The disks are readable on both PC and MAC systems (*i.e.*, the data was written to disk in standard ISO 9660 format). A set of CDs consists of ~12 individual disks, the last of which also contains a complete copy of the M&D database as of the time of

270

this writing. Copies of these CDs are available on a temporary loan basis from the LDEF Curator (*i.e.,* M.E. Zolensky) at JSC.

The LDEF Science Office located at Langley Research Center, Hampton, Virginia is considering CD-ROM storage of the on-orbit LDEF survey and general-view type pictures, as well as the post-flight deintegration and experiment tray stand pictures, for the purpose of long-term archiving and general access. The exact format in which these later files will be written to CD has not been determined. However, once completed these images will be available via computer link or on a temporary loan basis for interested workers. Finally, along these same lines, the M&D SIG presently plans to archive all LDEF M&D data it can acquire on CDs. However, this will only occur if the various LDEF investigators provide the M&D SIG with their data.

M&D SIG Report

The M&D SIG is in the process of putting together a report summarizing all M&D LDEF results and what they mean to the survivability of both manned and unmanned spacecraft in LEO. This report will include recommendations for further M&D-type activities and investigations on future spacecraft, as well as a long-term outlook as to ways in which the population of LEO particles can be monitored, as well as possible mitigation of its orbital-debris components.

Future Activities

Although FY 94 will conclude the initial LDEF activities, it will not mean an end to M&D-type studies and investigations. At the recently held 3rd LDEF Post-Retrieval Symposium in Williamsburg, Virginia, NASA Headquarters and the LDEF Science Office presented plans for the formation of a Space Environments & Effects (SEE) program. This program would encompass the various LDEF SIGs, as well as private industry and academia, and would be a customer-oriented program, focusing on issues related to designing, placing and safely maintaining both manned and unmanned payloads into Earth orbit.

REFERENCES

1) See, T.H., Mack, K.S., Warren, J.L., Zolensky, M.E., and Zook, H.A. (1993) Continued Investigation of LDEF's Structural Frame and Thermal Blankets by the Meteoroid & Debris Special Investigation Group. *LDEF - 69 Months in Space, Second LDEF Post-Retrieval Symposium, NASA CP-3194*, p. 313-324.

2) Hörz, F., Cintala, M.J., Bernhard, R.P., Cardenas, F., Davidson, W., Haynes, G., See, T.H., Winkler, J. and Knight, J. (1994) Cratering and Penetration Experiments in Teflon Targets at Velocities From 1 to 7 km/s. *NASA Technical Memorandum*, in press.

3) Kessler, D.J. (1991) Orbital Debris Environment for Spacecraft in Low Earth Orbit, *J. Spacecraft, 28, 3*, p. 347-351.

4) Zook, H.A. (1991) Meteoroid Directionality on LDEF and Asteroidal Versus Cometary Sources (abstract). *Lunar Planet. Sci. XXII*, Lunar and Planetary Institute, Houston, Texas., p. 1577-1578.

) Cour-Palais, B.G. (1987) Hypervelocity Impacts in Metals, Glass, and Composites, *Int. J. Impact Eng., 5*, p. 681-692.

5) See, T.H., Allbrooks, M.A., Atkinson, D.R., Simon, C.G. and Zolensky, M. (1990) *Meteoroid and Debris Impact Features Documented on the Long Duration Exposure Facility, A Preliminary Report, Publication #84, JSC #24608*, 583 pp.

7) See, T.H., Hörz, F., Zolensky, M.E., Allbrooks, M.K., Atkinson, D.R. and Simon, C.G., (1992) Meteoroid and Debris Special Investigation Group Preliminary Results: Size-Frequency Distribution and Spatial Density of Large Impact Features on LDEF. *LDEF - 69 Months in Space, First LDEF Post-Retrieval Symposium, NASA CP-3134*, p. 477-486.

8) Bernhard, R.P., See, T.H., Hörz, F. and Brownlee, D.E. (1994) Natural and Orbital Debris Particles on LDEF'S Trailing and Forward-Facing Surfaces, *LDEF - 69 Months in Space, Third LDEF Post-Retrieval Symposium, NASA CP-3275*, 1995.

9) Humes, D. (1994) Small Craters on the Meteoroid and Space Debris Experiment. *LDEF - 69 Months in Space, Third LDEF Post-Retrieval Symposium, NASA CP-3275*, 1995.

10) McDonnell, J.A.M. and Stevenson, T.J. (1992) Hypervelocity Impact Microfoil Perforations in the LEO Space Environment (LDEF, MAP A0023 Experiment). *LDEF - 69 Months in Space, First LDEF Post-Retrieval Symposium, NASA CP-3134*, p. 443-458.

11) Zook, H.A., (1992) Deriving the Velocity Distribution of Meteoroids From the Measured Meteoroid Impact Directionality on the Various LDEF Surfaces. *LDEF - 69 Months in Space, First LDEF Post-Retrieval Symposium, NASA CP-3134*, p. 569-579.

12) Kessler, D.J., (1993) Origin of Orbital Debris Impacts on LDEF's Trailing Surfaces. *LDEF - 69 Months in Space, Second LDEF Post-Retrieval Symposium, NASA CP-3194*, p. 585-594.

13) Coombs, C., Watts, A., Wagner, J. and Atkinson, D. (1992) *LDEF Data: Comparisons with Existing Models*. A final report to the M&D SIG under subcontract NAS9-17900, SC-02N0165768 to Lockheed - ESC.

14) Bernhard, R.P. and Zolensky, M.E (1994) Analytical Electron Microscopy of LDEF Impactor Residues. *LDEF - 69 Months in Space, Third LDEF Post-Retrieval Symposium, NASA CP-3275,* 1995.

15) Warren, J.L., Zook, H.A., Allton, J.H., Clanton, U.S., Dardano, C.B., Holder, J.A., Marlow, R.R., Schultz, R.A., Watts, L.A., and Wentworth, S.J. (1989) The Detection and Observation of Meteoroid and Space Debris Impact Features on the Solar Max Satellite, *Proc. Lunar Planet. Sci. Conf., 19th,* p. 641-657.

16) See, T.H., Allbrooks, M.K., Atkinson, D.R., Sapp, C.A., Simon, C.G., and Zolensky, M.E. (1992) Meteoroid & Debris Special Investigation Group: Data Acquisition Procedures. *LDEF - 69 Months In Space. First Post-Retrieval Symposium, NASA CP-3134,* p. 459-476.

17) Sapp, C.A., See, T.H., and Zolensky, M.E. (1992) 3-D Crater Analysis of LDEF Impact Features From Stereo Imagery, *LDEF - 69 Months In Space. Second Post-Retrieval Symposium, NASA CP-3194,* p. 339-345.

18) Press, W.H., et. al. (1987) *Numerical Recipes,* p. 289-293.